JACS
JOURNAL OF THE AMERICAN CHEMICAL SOCIETY
Article
Cite This: J. Am. Chem. Soc. 2019, 141, 5699−5709
pubs.acs.org/JACS

Activation of C−H, N−H, and O−H Bonds via Proton-Coupled Electron Transfer to a Mn(III) Complex of Redox-Noninnocent Octaazacyclotetradecadiene, a Catenated-Nitrogen Macrocyclic Ligand

Shivaiah Vaddypally,[†] Warren Tomlinson,[‡] Owen T. O'Sullivan,[†] Ran Ding,[†] Megan M. Van Vliet,[†] Bradford B. Wayland,[†] Joseph P. Hooper,*[,‡] and Michael J. Zdilla*[,†]

[†]Department of Chemistry, Temple University, 1901 North 13th Street, Philadelphia, Pennsylvania 19122, United States
[‡]Department of Physics, Naval Postgraduate School, 833 Dyer Road, Monterey, California 93943, United States

Supporting Information

ABSTRACT: Reaction of 1,3-diazidopropane with an electron-rich Mn(II) precursor results in oxidation of the metal center to a Mn complex with concomitant assembly of the macrocyclic ligand into the 1,2,3,4,8,9,10,11-octaazacyclotetradeca-2,9-diene-1,4,8,11-tetraido (OIM) ligand. Although describable as a Werner Mn(V) complex, analysis by X-ray diffraction, magnetic measurements, X-ray photoelectron spectroscopy, cyclic voltammetry, and density functional theory calculations suggest an electronic structure consisting of a Mn(III) metal center with a noninnocent OIM diradical ligand. The resulting complex, (OIM)Mn(NH^{t}Bu), reacts via proton-coupled electron transfer (PCET) with phenols to form phenoxyl radicals, with dihydroanthracene to form anthracene, and with (2,4-di*tert*-butyltetrazolium-5-yl)amide to extrude a tetrazyl radical. PCET from the latter generates the isolable corresponding one-electron reduced compound with a neutral, zwitterionic axial 2,4-di*tert*-butyltetrazolium-5-yl)amido ligand. Electron paramagnetic resonance and density functional theoretical analyses suggest an electronic structure wherein the manganese atom remains Mn(III) and the OIM ligand has been reduced by one electron to a monoradical noninnocent ligand. The result indicates PCET processes whereby the proton is transferred to the axial ligand to extrude ^{t}BuNH$_2$, the electron is transferred to the equatorial ligand, and the central metal remains relatively unperturbed.

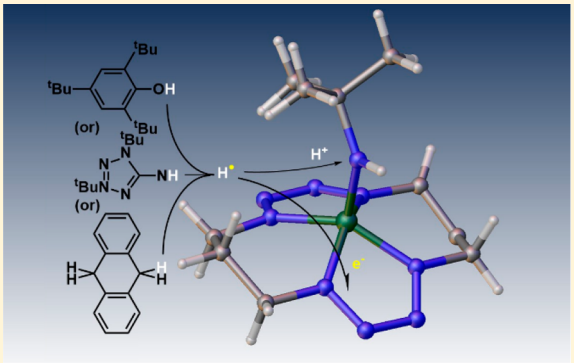

INTRODUCTION

Novel ligand platforms to mediate difficult redox reactions are of interest for synthetic homogeneous catalytic systems as well as biomimetic studies. Due to its prevalence in biological redox metalloenzymes,[1−3] the reactivity of Mn in various ligand platforms is a frequent subject of study.[4−13] In these systems, proton-coupled electron transfer (PCET)—the coordinated (but not necessarily simultaneous) movement of electrons and protons between reactants and products—is of central interest in a number of industrially and biologically relevant reactions mediated by transition metals.[14−18] In addition to the study of biomimetic reaction chemistry at Mn, our group has a particular interest in nitrogen-rich analogues of classical ligands with the goal of generating novel, metal-containing energetic materials.[19−22] We have previously reported on the assembly of the first manganese complexes of tetrazene, the N_4 analogue of the classic redox-noninnocent α-diimine ligand (Figure 1).[23]

Tetrazene complexes at metal centers are well established,[24−37] and formation most commonly occurs by the assembly of pairs of organic azides about the metal center with extrusion of N_2.[23,31,34,35] In addition to our own previous report on manganese,[23] noninnocent behavior in iron tetrazene complexes from several other groups are worthy of note.[36−38]

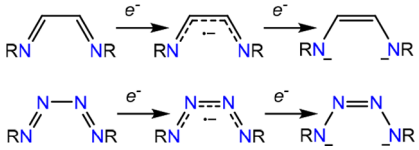

Figure 1. Analogy between redox noninnocent α-diimine (top) and tetraazadiene (bottom).

The vast majority of tetrazene complexes exhibit only a single tetrazene ligand, with only a few exceptions to our knowledge where complexes of two tetrazene ligands have been reported.[23,38] In this report, we describe a related assembly of a pair of tetrazene units embedded in a macrocyclic ligand around manganese, using as a synthon the disubstituted 1,3-diazidopropane. The result is a novel 1,2,3,4,8,9,10,11-octaazacyclotetradeca-2,9-diene-1,4,8,11-tet-

Received: September 21, 2018
Published: March 11, 2019

DOI: 10.1021/jacs.8b10250
J. Am. Chem. Soc. 2019, 141, 5699−5709

raido macrocycle (OIM) ligand, an octanitrogen topological analogue of the previously reported 2,3,9,10-tetraazacyclotetradeca-1,3-diene macrocycle (TIM),[39] and a redox noninnocent, unsaturated variant of the extensively reported tetraazacyclotetradecane (Cyclam) ligand.[40−45] This ligand also represents a more saturated analogue of the tetraazaannulene ligand and derivatives thereof, which has been a focus of our work[46−48] and that of others, including examples of manganese chemistry.[49−53] We report the synthesis of manganese complexes of OIM, their electronic structures, and PCET reactions via activation of C−H, N−H, and O−H bonds.

RESULTS AND DISCUSSION

Synthesis and Characterization of 1 and 2. We have previously shown that coordination of Mn(II) precursors in situ by the strong σ-donor *tert*-butyl amide destabilizes the low oxidation state, favoring metal oxidation.[23,54,55] Reaction of 1,3-diazidopropane[56] with a mixture of bis[bis(trimethylsilyl)-amidomanganese(II)[57] and excess *tert*-butyl amine results in assembly of a formally manganese(V) Werner complex of the OIM ligand with an apical *tert*-butylamido ligand, (OIM)-$Mn^{V}(NH^{t}Bu)$ (**1**, Scheme 1, Figure 2) in 50% yield. The OIM ligand presumably forms from the well-established[23,31,34,35] condensation of two azides into tetrazene with concomitant extrusion of N_2 (Scheme 1). X-ray crystallographic analysis (Table 1) shows that the central N−N bond on each side of the macrocycle is slightly shorter (1.28−1.29 Å) than the outer N−N bonds (1.32−1.34 Å). Such a "long-short-long" pattern is often associated with the fully reduced oxidation state of this potentially redox-noninnocent ligand,[58] though these particular bonds are all still in an intermediate range between the expected lengths of N−N single (∼1.47 Å) and double (∼1.24 Å) bonds, suggesting the possibility of redox-noninnocent radical character on the ligands. Further, N−N bond lengths are not a conclusive measure of ligand redox state,[59] and more thorough electronic structure investigation is warranted.

Scheme 1

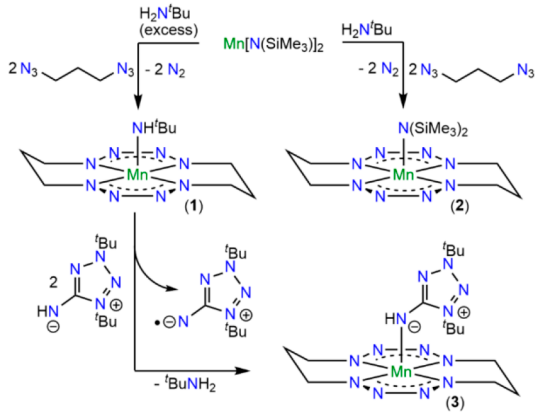

The apical ligand is assigned as a protonated amide ligand based upon the apical bond length between Mn and the *tert*-butylamide nitrogen of 1.788 Å, signifying a monoanionic apical ligand with partial double-bond character. Further, the presence of an N−H stretch at 3200 cm^{-1} in the infrared spectrum signifies the presence of an amide proton, as does the successful crystallographic refinement of a single proton on the apical amido nitrogen atom. While charge balance suggests a formal oxidation state of Mn(V), this is a relatively uncommon

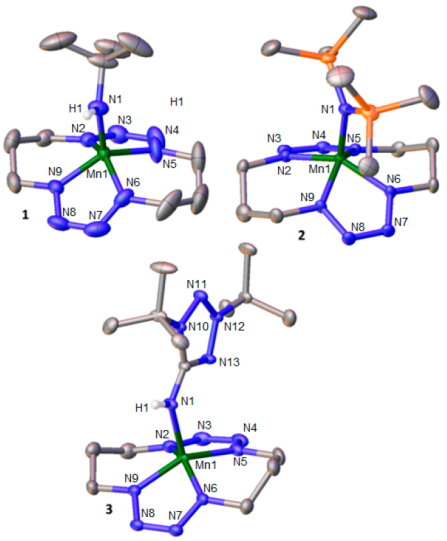

Figure 2. Thermal ellipsoid plots of (OIM)Mn(L) complexes. Ellipsoids set at 50% probability level. C−H hydrogen atoms omitted for clarity. **1**, L = $[NH^{t}Bu]^{-}$; **2**, L = $[N(SiMe_3)_2]^{-}$; **3**, L = $NH(CN_4{}^{t}Bu_2)$.

oxidation state. Even more uncommon is an isolable Mn(V) complex without a terminal multiply bonded imide, oxide, or nitride ligand.[5,60−64] Compound **1** does not have a discernible NMR spectrum, suggesting the resonances are relaxed by a paramagnetic metal center. Evans method magnetic measurements gives a μ_{eff} of 2.37 Bohr magneton, most consistent with a high-spin $S = 1$ system (spin only value of μ_{eff} = 2.83 Bohr magneton). In acetonitrile-d_3 solution, interaction of the acetonitrile residual protiosolvent with the open axial coordination site in a 20 mM solution of **1** relaxes the protiosolvent pentet to a singlet, suggesting a fast-relaxing, and rapidly fluctuating magnetic $S = 1$ system. Mn(V) complexes in analogous planar macrocyclic templates are most frequently low-spin due to high-lying d_{xz} and d_{yz} orbitals in the presence of strongly π-donating axial ligands. In this system, such a triplet electronic state is less common.[65] An electron paramagnetic resonance (EPR) signal in parallel mode was not seen, which may be due to large zero-field splitting. However, the existence and magnitude of 3s splitting in the Mn X-ray photoelectron spectroscopy (XPS) provides spectroscopic support for the spin state assignment (vide infra). Compound **1** has a low reduction potential of −718 mV vs ferrocene as evidenced by a quasireversible signal in the cyclic voltammogram (see Supporting Information). For a metal-based reduction of a Mn(V) ion, a higher reduction potential would be expected. For instance, even with high-oxidation-state-stabilizing corrolazine ligand and triply bonded axial oxo ligands, the Mn(V)═O system of Goldberg was reported to have a reduction potential ∼320 mV higher[66] than **1**. The low reduction potential of **1** thus suggests the reduction event may not occur at a Mn(V) ion, and may not even be metal-based. The preponderance of unusual features for a Mn(V) mononuclear system suggests the likelihood that the complex is better described by an alternative valence tautomer, and that the redox noninnocent ligand may hold one or more redox equivalents.

An analogous synthesis performed with a smaller, stoichiometric amount of *tert*-butylamine resulted in the isolation of the analogous compound with an apical trimethylsilylamido

DOI: 10.1021/jacs.8b10250
J. Am. Chem. Soc. 2019, 141, 5699−5709

Table 1. Selected Bond Lengths (Å) from (OIM)$Mn^{V}(NH^{t}Bu)$ (1), (OIM)$Mn^{V}(N(SiMe_3)_2)$ (2), and (OIM)$Mn^{IV}(NH(CN_4{}^{t}Bu_2)$ (3)[a] from Single-Crystal XRD and DFT Calculations

	1	1 (DFT)[b]	2	3	3 (DFT)[b]
Mn(1)−N(1)	1.786(4)	1.873	1.859(2)	1.9567(19)	2.198
Mn(1)−N(2/5)	1.851(3)/1.850(4)	1.869/1.877	1.874(2)/1.861(2)	1.844(2)/1.860(2)	1.877/1.877
Mn(1)−N(6/9)	1.853(4)/1.848(3)	1.875/1.881	1.867(2)/1.864(2)	1.848(2)/1.8598(19)	1.892/1.892
N(3/7)−N(4/8)	1.281(6)/1.290(6)	1.299/1.303	1.300(3)/1.301(3)	1.302(3)/1.299(3)	1.271/1.291
N(2/4)−N(3/5)	1.327(5)/1.333(6)	1.310/1.306	1.338(3)/1.336(3)	1.349(3)/1.338(3)	1.339/1.339
N(6/8)−N(7/9)	1.328(6)/1.336(5)	1.304/1.305	1.340(3)/1.337(3)	1.353(3)/1.349(3)	1.319/1.319

[a]Divided entries refer to separate, related atoms and their associated metrics in the order given, e.g., N(3/7)−N(4/8) denotes two bonds: N(3)−N(4) and N(7)−N(8). [b]Structures optimized using the MN15 functional and aug-cc-pVTZ basis set.

ligand in place of *tert*-butyl amide, (OIM)$Mn^{V}(N(SiMe_3)_2)$ (**2**, Scheme 1, Figure 2) albeit in only trace yields. Bond metrics in the macrocyclic **2** for the inner and external N−N bonds (1.29−1.30 and 1.33−1.35 Å, respectively) are similar to those in **1** (Table 1) again suggesting possible intermediate N−N bond order, though the apical Mn−N bonds are slightly longer, at 1.84−1.86 Å, but still indicative of a monoanionic axial nitrogen.

Given the unusual spin state and structural features in these compounds, we examined the electronic structure of the manganese atom in more detail using XPS to measure the binding energies of the core 2p electrons and the 3s electronic splitting, which are often invoked as a means to identify manganese oxidation state. In this analysis, higher oxidation states correspond to larger 2p electron binding energies and smaller 3s electronic splitting, for instance, in manganese oxides.[67] The complexes presented here are not oxides, however, and the covalency of the metal ligand bond does slightly affect the position of the 2p signals, with increased M−L covalency tending to decrease binding energy.[68] The $^{3/2}$2p XPS peak of **1** occurs at 641 eV (Figure 3) and its low energy and shape are inconsistent with Mn(IV) or higher oxidation states.[67] While this value of binding energy is also slightly low for Mn(III) oxides, the absence of the satellite shakeup feature at 647 eV suggests it is not assignable as Mn(II).[67] The signal

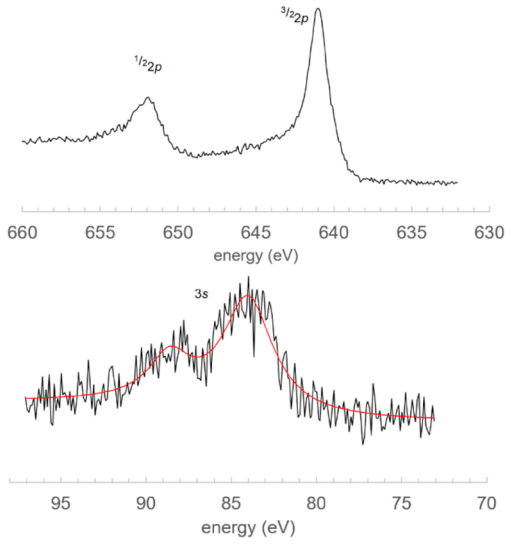

Figure 3. XPS spectra showing ionization potentials of core manganese electrons. Top: 2p spectral region, showing diagnostic $^{3/2}$2p signature at 641 eV. Bottom: 3s spectrum (black) with two-Lorentzian fit (red) showing an approximate 3s electronic splitting of 4.6 eV.

is thus most consistent with a Mn(III) ion whose donor ligands are stronger than oxide; similar ionization energies have been seen for Mn(III)-acetonylacetate-type complexes with electron-rich (*tert*-butyl) donating groups on the ligand periphery,[68] and for surface Mn(III)-nitride species.[69] The spectrum is thus an excellent match to the expected position for nitrogen-ligated Mn(III) in **1**. Correspondingly, fitting of the $^{3/2}$2p spectra to the expected multiplet patterns in Mn according to the method of Nesbitt[70] gave a superior fit for Mn(III) (see SI). The assignment of a Mn(III) metal center therefore suggests a partially oxidized dianionic diradical OIM ligand.

The splitting of the Mn 3s XPS signal is related to the number of unpaired electrons and is frequently cited as another measure of manganese oxidation state. Despite poor signal-to-noise ratio in the 3s region of the spectrum, a splitting of approximately 4.6 eV is measurable (Figure 3), somewhat lower than the expected splitting (5.5 eV) in Mn(III) oxide calibrants and closer to the value of Mn(IV) calibrants.[71] This discrepancy is explainable by virtue of the experimental $S = 1$ spin state of **1**, which arises from proposed redox non-innocence in the ligands of **1**. This is in contrast to Mn^{III}−O calibrants, for which electronic spin is relegated entirely to the metal ion, and the spin state is $S = 2$. The 3s splitting is the result of two possible ionization products in paramagnetic manganese ions resulting from the ionization of either the α- or the β-3s electron, which gives a product with the remaining 3s electron either paired with the 3d electrons (Hund-type system) or against (non-Hund). Thus, the value of 3s splitting is largest for traditional $S = 5/2$ weak-field Mn(II) complexes[71] due to the increased exchange energy for the spin-aligned Hund-type product and the increased electron−electron repulsion for the non-Hund product. In Mn−O calibrants, this splitting decreases as the Mn atom is oxidized to higher oxidation states due to the corresponding decrease in spin quantum number and resultant decreased exchange energy for the Hund-like configuration, and decreased electron−electron repulsion for the non-Hund configuration. However, since compound **1** is not a traditional $S = 2$ Werner-type Mn(III) complex with closed-shell ligands, but rather a paramagnetic complex with an open-shell redox noninnocent ligand, the normal expectations for the 3s splitting will not necessarily hold if the ligand based singly occupied molecular orbital (SOMO) orbitals have significant metal character. The measured spin state of $S = 1$ based on solution magnetic susceptibility suggests the ligand radicals are antiferromagnetically coupled to the metal center. This decreased overall spin is expected to decrease the 3s splitting due to lower exchange energy, which explains the low measured splitting of 4.6 eV. Thus, the 3s and 2p regions of the Mn XPS are consistent with

DOI: 10.1021/jacs.8b10250
J. Am. Chem. Soc. 2019, 141, 5699−5709

a Mn(III) ion antiferromagnetically coupled to ligand-based radicals. Further, these observations provide a precautionary tale on the use of 3s splittings to assign metal oxidation states in complexes with redox noninnocent ligands: 3s splitting in noninnocent complexes cannot be directly compared to Mn−O calibrants due to differences in quantum spin.

Density Functional Theoretical Calculations on 1. While **1** might be formally described as a Mn(V) complex with a dianionic tetrazadiene ligand, several unusual experimental features discussed above suggest this description may be electronically invalid. These observations include the absence of a strongly π-donating axial ligand, an unusual S = 1 electronic spin state, OIM N−N bond lengths indicative of intermediate bond order, and XPS spectra all suggestive of the possibility of ligand redox noninnocent behavior. For further support we examined the electronic structure using density functional theoretical methods. The structure of **1** was calculated in the gas phase with the unrestricted MN15 functional and a triple-ζ aug-cc-pVTZ basis set. A number of physical parameters, notably the spin density localized on the Mn and the Mn-apical N bond length, are sensitive to the functional and basis set. The Supporting Information[72,73] provides full details about the downselection of a computational method; the Minnesota family of functionals with a large percentage of exact exchange and a large triple-ζ basis set were found to be the most accurate for these systems. Accordingly, the MN15/aug-cc-pVTZ combination is used for all calculations presented here. Details are also given in the SI on the examination of alternative spin states, which are closely energetically spaced. Calculated bond lengths for **1** are generally consistent with X-ray data (Table 1) with the exception of the Mn(1)−N(1) apical bond. All density functional theory (DFT) methods examined overpredicted its length, and thus as a check, electronic structure calculations were also performed for all systems fixed at the experimental X-ray geometry. Calculated N−N bond lengths in OIM otherwise agree reasonably well with experiment and support an intermediate state between N−N single and double bonds.

Mulliken spin density and topological analysis suggest that **1** is best described as an Mn(III) center with an overall S = 1 spin state and noninnocent features on the OIM ligand. The calculated spin density for the Mn atom in the optimized complex is +3.88 e^-, consistent with a d^4 Mn^{III} ion, and corresponding spin density plots are shown in Figure 4. A small amount of spin (+0.03 e^-) has delocalized from the Mn onto the apical N. Close to 2 e^- of unpaired β-electron density is localized on the four nitrogens of the OIM ligand. When fixed in the experimental geometry, the α-spin density on the metal decreases slightly to +3.64 e^-. Biorthogonalized orbital analysis was conducted and indicates the presence of four predominately d-character α-SOMO orbitals, consistent with a d^4 Mn(III) ion. Figure 5 shows the energies of these four orbitals relative to the highest-occupied molecular orbital (HOMO) for the complex.

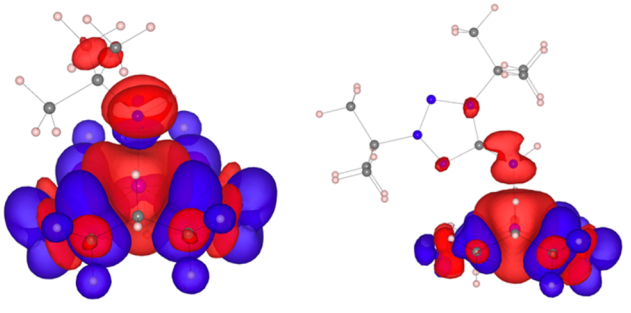

Figure 4. Spin density plots of **1** (left) and **3** (right).

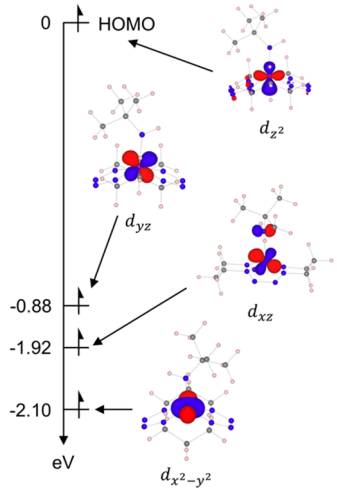

Figure 5. Four singly occupied d-character orbitals in **1**.

The electron localization function (ELF)[74] is a useful analysis for the visualization of bonding and the assignment of oxidation state. The ELF takes advantage of the Pauli exclusion principle to assign basins with high probability of paired electrons, which correspond to the locations of bonds, nonbonding "lone pairs", or core electrons, offering an analogy to Lewis theory. Further, the electron count within these basins can serve as a computationally rigorous analog of traditional electron counting approaches in inorganic chemistry used for oxidation state assignment. The ELF for **1** (Figure 6) also supports a Mn(III) oxidation state. In complex **1** there are five disynaptic valence basins between Mn and the ligand nitrogen atoms (Figure 6, green), which may be considered as bonds, along with a single monosynaptic valence basin on the apical N representing a nitrogen lone pair (Figure 6, blue). However, there is significant overlap between the mono- and disynaptic basins, and all are located between the Mn and the five nearest nitrogens; this suggests these are all participating in the bonding process.

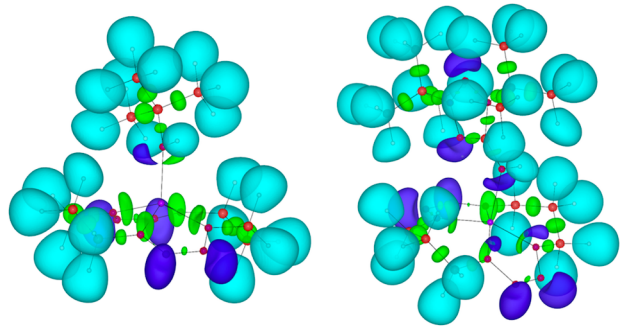

Figure 6. ELF for **1** (left) and **3** (right). The f = 0.88 isosurface is shown. Core electron basins are shown in red, protonated valence basins in cyan, monosynaptic basins (lone pairs) in blue, and disynaptic valence basins (bonds) in green.

DOI: 10.1021/jacs.8b10250
J. Am. Chem. Soc. 2019, 141, 5699−5709

All six basins mentioned above appear to contribute to N−Mn bonding and are significantly shifted away from the central metal toward the nitrogen atoms. This, combined with the lone pair character of the monosynaptic basin, suggests that the bulk of the electron density within the basins is associated with the nitrogen atoms. Thus, to a first approximation, all electrons in these basins may be considered as either lone pairs or as ligand donor pairs coordinating to the metal ion. The total population within these six basins in **1** is 17.72 e^-. Considering that each of the five nitrogen atoms provides three valence electrons to be paired in covalent bonds (15 total), then these population counts indicate that the Mn has transferred 17.72 − 15 = 2.72 e^- to the five ligand nitrogens in **1** and thus has a formal charge of +2.72, consistent with a Mn(III) metal center.

PCET Reactions. Reactivity tests demonstrate **1** is capable of formally abstracting C−H, N−H, and O−H hydrogen atoms from substrates with relatively weak X−H bonds, resulting in reduction of the metal complex by a single electron and concomitant protonation and labilization of the axial *tert*-butyl-amide ligand as an amine. Motivated by our work in novel energetic materials, we sought to generate a metal coordination complex with greater nitrogen content by replacement of the axial *tert*-butylamido ligand of **1** with a nitrogen-rich tetrazolate ligand. The neutral, zwitterionic(1,3-di-*tert*-butyl-1*H*-tetrazol-3-ium-5-yl)amide reagent[75] was intended to protolyze the axial *tert*-butylamido ligand, releasing it as *tert*-butylamine, and resulting in simple ligand exchange to give the isovalent manganese complex with axially ligated (1,3-di-*tert*-butyl-1*H*-tetrazol-3-ium-5-yl)imide. Instead, a PCET reaction ensued, as evidenced by the appearance of detectable 1,3-di-*tert*-butyl-1*H*-tetrazol-3-ium-5-yl radical by EPR spectroscopy (Figure S4), the expected product of hydrogen atom abstraction (Scheme 1). Density functional theoretical calculations on this di-*tert*-butyltetrazolamide substrate (MN15/aug-cc-pVTZ) indicate a bond dissociation free energy of 419 kJ/mol at 298 K, higher than that of 2,6-di-*tert*-butylphenol (399 kJ/mol)[76] as expected due to it being a stronger N−H bond and electron-enriched due to its monoanionic protonation state.

As compound **1** was able to activate the N−H bond of the aminotetrazole substrate, further substrate tests were performed to explore what other bond types could be activated by PCET. As expected, tri-*tert*-buyl phenol, a common arene-based PCET substrate,[77−81] was converted to the phenoxyl radical by reaction with **1** as detected by EPR spectroscopy (Figure S5). Finally, the possibility of C−H activation by compound **1** was explored by reaction with excess dihydroanthracene. Gas chromatographic analysis of the reaction product mixture shows the formation of anthracene, in 40% yield based on **1**, confirming the ability of **1** to activate the C−H bond of dihydroanthracene (Figure S6). Other C−H bond activation at high-valent manganese−oxygen[82−86] and manganese−imido[87−89] systems are worthy of note. Our system is unusual in that it represents an example of a hydrogen atom transfer to an amido (not imido) ligand to form an amine-based product, *tert*-butyl amine.

Characterization of Product 3. Instead of the intended ligand-exchanged product, the formally manganese(IV) complex, with a protonated, neutral (zwitterionic) tetrazolamido ligand, (OIM)Mn[NH($CN_4{}^tBu_2$)] (**3**, Figure 2), was isolated from the reaction of **1** with di-*tert*-butyltetrazoliumamide. The protonated state of the tetrazole ligand is evidenced by the identification and successful refinement of a proton on the apical amide nitrogen, and the relatively long contact with the metal atom at 1.96 Å in comparison with the shorter apical bonds in compounds **1** and **2** (1.79 and 1.86, respectively). The bond lengths for the interior and exterior N−N bonds of the macrocyclic OIM ligand are similar (1.3 and 1.34−1.35 Å, respectively) to those of **1** and **2**, though longer on average, signifying possible reduction of the OIM ligand. The intermediate values of the N−N bond lengths again suggest the possibility of an intermediate redox state of the ligands, though bond lengths alone are a poor indicator of exact ligand redox state.[59] With the neutral zwitterionic axial ligand, the reaction stoichiometry suggests a one-electron reduction has occurred concomitant with the protolytic removal of *tert*-butyl amide (Scheme 1).

The generation of this protonated, one-electron reduced complex from NH($CN_4{}^tBu_2$) suggests the involvement of two equivalents of the tetrazole reagent with different roles (Scheme 1): half of the reagent performs a PCET reaction whereby the tetrazolylamido proton protolyzes *tert*-butyl amide, releasing it as *tert*-butylamine and extrudes a tetrazolyl radical, providing a single electron and reducing the complex. The organic byproduct, tetrazolyl radical, is analogous to common aromatic radicals formed from phenols or aryl amines[77−81] and is detectable by EPR (Figure S4). To our knowledge, this is the first example of a metal-mediated PCET reaction at a tetrazole, though reports of stable tetrazolyl radicals exist.[90−92] The remaining half of the tetrazole-based reagent, being a stronger-donating zwitterionic amide ligand, simply replaces the now labile *tert*-butyl amine ligand, and coordinates the Mn atom, giving compound **3** in 42% yield according to eq 1:

$$(\mathrm{OIM})\mathrm{Mn}^{\mathrm{V}}(\mathrm{NH}^t\mathrm{Bu}) + 2\mathrm{NH}(\mathrm{CN}_4{}^t\mathrm{Bu}_2) \rightarrow (\mathrm{OIM})\mathrm{Mn}^{\mathrm{IV}}(\mathrm{NH}(\mathrm{CN}^t\mathrm{Bu}_2) + (\mathrm{CN}_4{}^t\mathrm{Bu}_2)\mathrm{N}\cdot + {}^t\mathrm{BuNH}_2 \quad (1)$$

Compound **3** is a high-spin $S = 3/2$ system based upon its EPR spectrum, which shows a rhombically distorted axial signature (Figure 7). This spin state is possibly consistent with a Mn(IV) d^3 complex; however, our past characterization of a related manganese tetrazene complex[23] also exhibited a $S = 3/2$ signature but was better described as a Mn(III) complex with a delocalized ligand radical. Though this previously reported EPR signature exhibited a very different shape than that in Figure 7, this is to be expected due to a different pseudotetrahedral coordination geometry than that of square pyramidal **3**. Thus, as in the case of **1**, the electronic structure warrants careful investigation.

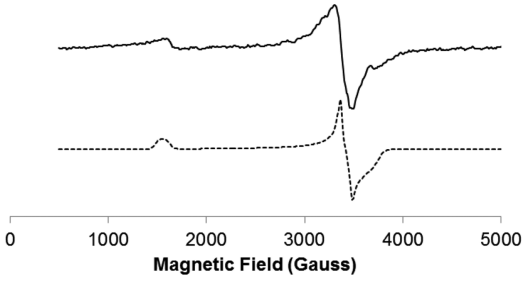

Figure 7. Experimental and simulated EPR spectra of **3**: gx = 1.90, gy = 2.01, gz = 4.43; MW Freq., 9.633014 GHz; MW power, 20.12 mW; Mod. Freq., 100 kHz; Mod. Amplitude, 6.00 G.

DOI: 10.1021/jacs.8b10250
J. Am. Chem. Soc. 2019, 141, 5699−5709

Density Functional Theoretical Calculations on 3. While the ground spin state of **3** is consistent with a simple Mn(IV) tetrazene complex with a dianionic tetrazene ligand (Figure 1-left), it is worth noting that, like in the case of **1**, the N−N bond lengths in the OIM ligand, though they exhibit the expected long−short−long (1.34−1.30−1.35 Å) pattern of the fully reduced ligand, possess values in an intermediate range between the expected lengths of N−N single (∼1.47 Å) and double (∼1.24 Å) bonds, suggesting the possibility of redox-noninnocent radical character on the ligands. This would be consistent with our former report of a four-coordinate neutral manganese bistetrazene complex, which was described as a Mn(III) ion with delocalized radical character on the ligands.[23]

Like **1**, compound **3** was optimized with the unrestricted MN15 functional and the triple-ζ aug-cc-pVTZ basis set. Mulliken spin density and molecular orbital analysis indicate that the manganese atom in **3** (like in **1**) is most consistent with a Mn(III) oxidation state with a delocalized ligand radical. Calculated spin density on the Mn atom is +4.40 e^-, comparable to the value of +3.88 e^- for **1**, but slightly higher due to overall reduction of the molecule, but still consistent with a d^4 Mn(III) ion. Spin density plots are shown in Figure 4. A small amount of spin (+0.02 e^- for **3**) has delocalized from the Mn onto the apical N. As expected, the delocalization is smaller in **3** than in **1** due to the increased bond length (2.20 vs 1.87 Å). Roughly 1 e^- of β-electron density is present on the four nitrogens adjacent to the Mn on the OIM ligand. Calculations fixed in the experimental geometry show a spin density on the Mn atom of +4.37, very close to the value calculated at the optimized geometry.

As in the case with **1**, biorthogonalized orbital analysis was conducted and indicates the presence of four predominately d-character singly occupied orbitals for both **1** and **3**, consistent with a description of a Mn(III) center for both. The HOMO in both cases has predominately Mn d_{z^2} character. Thus, besides a reordering of the deeper-lying d-orbitals, the electronic structure at Mn remains surprisingly unperturbed following one-electron reduction. Figure 8 plots the energies of these four orbitals relative to the HOMO. Figure S10 compares the biorthogonalized orbitals of **1** and **3** side-by-side.

Quantum Theory of Atoms in Molecules (QTAIM) analysis is another useful tool for examining bonding environments in donor−acceptor complexes from quantum calculations.[93] QTAIM uses basins of electron density to assign bond critical points (BCPs) that reveal the locations and properties of bonds from electron density, the Laplacian of electron density, and energy density at these BCPs, and is particularly useful as a measure of bonding analogy between structurally similar complexes. QTAIM analysis reveals the presence of BCPs between the manganese atom and the five closest nitrogen atoms for both **1** and **3**. For **1**, density metrics at the BCPs indicate a weak, shared metal−ligand interaction with a negative energy density H_b and a positive electron density Laplacian $\nabla^2\rho_b$. The four Mn−N bonds in **3** connecting the metal to the OIM ligand are topologically almost identical to the five Mn−N bonds in **1**, demonstrating the electronic analogy between the two complexes, despite the differing formal oxidation state. The BCP connecting the metal to the apical nitrogen in the weaker $NHCN_4(^tBu)_2$ ligand, however, is different, as expected. The values for ρ_b and $\nabla^2\rho_b$ are reduced by a factor of 2, and H_b is reduced by nearly a factor of 4. While this bond is chemically similar to the other bonds, it is significantly weaker. Table 2 shows average metrics for the five Mn−N BCPs in **1** and the four Mn−N OIM BCPs in **3** as well as the metrics for the Mn-apical N BCP.

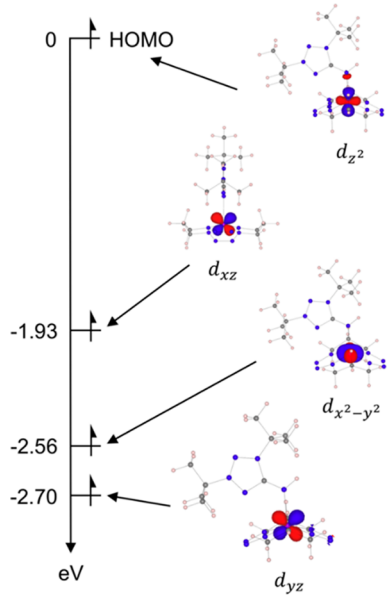

Figure 8. Four singly occupied d-character orbitals in **3**.

Table 2. QTAIM Metrics for Mn−N Bonds in 1 and 3[a]

BCPs	ρ_b	$\nabla^2\rho_b$	H_b
Mn−N (**1**)	0.1085	0.3888	−0.0353
Mn−N (**3**)	0.1151	0.3929	−0.0399
Mn−N1 (**3**)	0.0566	0.2180	−0.0101

[a]All values given in atomic units.

The ELF for **3** also supports a Mn(III) oxidation state. In **3**, there are four disynaptic valence basins (bonds) and three monosynaptic basins (lone pairs) between the metal and adjacent nitrogen atoms, and like in **1**, there is significant overlap between the mono- and disynaptic basins, and all are located between the Mn and the four nearest nitrogens; all are participating in the bonding process. Figure 6 displays the ELF for both complexes. As in **1**, all basins contribute to N−Mn bonding and are significantly shifted away from the central metal toward the nitrogen atoms, and the bulk of the electron density within the basins is associated with the nitrogen atoms. The total population within seven basins in **3** is 18.47 e^- (comparable to the total of 17.72 e^- in **1**). Subtraction of this value from the theoretical 15 valence electrons available among the 5 donor nitrogens gives a difference of 3.47 e^-, corresponding to a formal charge of +3.47 on nitrogen, also consistent with an Mn(III) metal center.

Between the comparable biorthogonalized orbitals, metal spin densities, bond metrics, ELF, and QTAIM analyses, the results are suggestive of a remarkably similar electronic structure at the Mn atom between complexes **1** and **3**, despite **3** being formally reduced by a full electron. Indeed, the spin- and charge-density changes upon reduction of **1** to **3** by PCET suggest that the reduction is centered on the redox noninnocent OIM ligand, not the metal center. Thus, the operative PCET process involves a mechanism where the proton is transferred to the axial *tert*-butyl amide ligand, and

DOI: 10.1021/jacs.8b10250
J. Am. Chem. Soc. 2019, 141, 5699−5709

the electron is transferred to the equatorial OIM ligand, with very little alteration of the electronic structure of the metal atom itself, as evidenced by spin-density, QTAIM, and ELF analysis. Related examples of hydrogen atom transfer reactions that do not involve redox changes at the metal include recent work on Ru(V) porhyrinoids from the Goldberg group[94] wherein a hydrogen atom is transferred to the porphyrin ligand without a change in oxidation number. Additionally, work in this group involved the transfer of hydrogen atoms to a valence tautomeric Mn(IV)-corrolazine radical cation where the electron reduces the corrolazine ligand, and the axial oxo ligand becomes protonated without a formal change in manganese oxidation state.[95] A related example from Abu-Omar exhibited two PCET events where only one of the two electrons reduces the metal center but both protons protonate the axial oxo ligand.[96]

CONCLUSION

We report here the synthesis of an unsaturated octaaza topological analogue of the TIM, Cyclam, and tetraazaannulene ligands: 1,2,3,4,8,9,10,11-octaazacyclotetradeca-2,9-diene-1,4,8,11-tetraido macrocycle (OIM). The ligand features two redox-noninnocent tetrazene-based bidentate ligand motifs within a 14-membered macrocycle. The formation of a pseudo square pyramidal motif is observed, with a formal oxidation state of Mn(V), which is better described as a Mn(III) complex with a partially oxidized OIM ligand diradical. PCET to this complex may be initiated by reaction with various weak O−H, N−H, or C−H donors. In the case of reaction with 2,4-di-*tert*-butyltetrazolium-5-yl)amide, isolated is a formal Mn-(IV) complex that forms by PCET. Electronic structure analysis indicates that this complex is also best described as an Mn(III) complex and that the reduction has occurred on the OIM ligand, with the proton being transferred to the axial amide ligand.

It is curious to note that, in combination with our previous report,[23] there now exist a total of five separate manganese tetrazene complexes over a range of three different oxidation state (formally between III and V), yet electronic structure analysis suggests that all complexes thus far reported are best described as Mn(III) complexes with varying ligand oxidation state. Future efforts will attempt to further elucidate the mechanism of PCET, including whether electron transfer precedes, coincides with, or follows proton transfer in this PCET with divergent proton and electron movement.

EXPERIMENTAL SECTION

Precautions. The low-carbon azide and tetrazene molecules are ***explosive*** materials. They should be stored cold in solutions of concentration of no more than 0.5 M or isolated only in few-milligram quantities. Shock, spark, heat, or, in the case of **3**, the exotherm from exposure to air can result in explosion. Weighing should be performed with a plastic spatula, with the experimenter electrically grounded by a wire attached to the wrist in contact with skin. Proper precautions should be taken, including use of standard laboratory PPE plus explosion proof mask, shield, Kevlar gloves, use of plastic spatulae, and electrical grounding while handling these materials. All syntheses were performed in microscale for maximum safety.

General Methods. All operations were performed under a rigorous dry, anaerobic atmosphere of nitrogen gas using standard Glove Box and Schlenk line techniques. All reagents were purchased from commercial sources (Aldrich, Strem). Anhydrous solvents such as acetonitrile and pentane were purified using an Innovative Technology, Inc. Pure Solv. system. Tetrahydrofuran and hexamethyldisiloxane were distilled from sodium benzophenone ketyl under a nitrogen atmosphere. $^{t}BuNH_2$ was purchased from Aldrich, and $Mn[N(SiMe_3)_2]_2$,[57] 1,3-diazidopropane,[56] and di^{t}butylamino-tetrazole[75] were synthesized according to literature protocol. Anhydrous solvents were used throughout all experiments. ^{1}H NMR spectra were recorded on a Bruker Avance 400 MHz spectrometer. FT-IR spectra were recorded in the range of 400−4000 cm^{-1} on a Nicolet iS5 FT-IR with a iD5 attenuated total reflectance (ATR) accessory. EPR spectra were recorded on a Bruker EMX X-band spectrometer equipped with an Oxford Cryosystems low temperature cryostat. Spectra were recorded at 5 K. UV−visible spectra were recorded on a Shimadzu UV-1800 UV spectrophotometer in the range of 200−900 nm. High resolution mass spectrometry was performed on an Agilent 6520 Accurate Mass Measurement Q-ToF mass spectrometer. Single crystal and powder X-ray diffraction were performed on a Bruker KAPPA APEX II DUO diffractometer. Single crystals were mounted on a MiTeGen loop using N-Apezion and powder XRD, and samples were caked onto the end of a glass fiber using N-Apezion. Crystal data was collected and processed using the Bruker Suite[97] and solved and refined using the SHELXTL suite[98] with Olex2 as a GUI.[99] CHN elemental analysis was carried out at Rochester University under the CENTC instrumental facility. XPS was performed using a Thermo Fisher K-Alpha+ with an Al−Kα monochromatic X-ray source. Data collected for the Mn $2p_{3/2}$ and O 1s spectral regions were peak-fitted using Casa XPS software. To fit the Mn $2p_{3/2}$ region the procedure used by Nesbitt[70] was employed, which takes into account the multiplet structure resulting from the presence of unpaired valence electrons in the 3d orbitals of manganese in the birnessite sample. This fitting procedure relies on the theoretical calculations by Gupta of the expected XPS spectra from the three Mn(IV), Mn(III), and Mn(II) ions.[100,101] The prior work showed that the calculated XPS spectra for the free ions (each containing 5 multiplet peaks) allowed the accurate fitting of experimental XPS Mn $2p_{3/2}$. Peaks with a 50:50 Gaussian/Lorentzian contribution were used in the procedure, and the full width half-maximum for each peak was between 0.79 and 1.57 eV. Using these parameters, the spectral data was fitted by varying the relative contribution of individual sets of multiplet peaks.

Synthesis. *Synthesis of [Mn(OIM)(HN^{t}Bu)] (**1**).* $Mn[N(SiMe_3)_2]_2$ (0.0375 g, 0.100 mmol) was dissolved in 5 mL of pentane and followed by addition of 1,3-diazidopropane (0.1 g, 0.8 mmol) resulting in a light-yellow solution. One milliliter of *tert*-butylamine was added to reaction mixture dropwise, which turned to a dark brown solution. This reaction mixture is stirred further for 2.5 h and filtered through a 0.45 PTFE syringe filter. The filtrate was recrystallized by vapor diffusion at room temperature in a double-vial apparatus with hexamethyldisiloxane as precipitant. Dark brown crystals are obtained after 5 days. The crystalline material was isolated by decanting the mother liquor and washing with pentane. Yield: 0.016 g (0.050 mmol); 50% based on $Mn[N(SiMe_3)_2]_2$. FT-IR: [cm^{-1}] 3204 (N−H stretch) 2943, 2844, (C−H stretch); 1421, 1394, 1336 (C−H bend) 1259, 1200 (M═R stretch). Unit Cell (XRD): orthorhombic *P*. a = 7.5991(15) Å, b = 9.5866(19) Å, c = 20.193(4) Å, V = 1471.1(5) Å^3. CHN analysis calcd for $C_{10}H_{22}MnN_9$: C, 37.153%; H, 6.859%; N, 38.994%. Found: C, 36.976%, H, 6.512%; N, 38.815%.

*Synthesis of [Mn(OIM)(N(SiMe$_3$)$_2$)] (**2**).* The synthesis of compound **2** is performed exactly as compound **1** except that only 100 μL of *tert*-butylamine was added. A solid, insoluble product was obtained from the reaction mixture after 1 day. The mother liquor was decanted, and the residue discarded. The mother liquor was transferred to a double apparatus with hexamethyldisiloxane as precipitant. A trace yield of light orange crystals is obtained in 2 days. Unit cell (XRD): triclinic *P*. a = 8.3841(11) Å, b = 15.402(2) Å, c = 17.081(2) Å, α = 73.318(3)°, β = 81.288(3)°, γ = 89.959(3)°, V = 2086.4(5) Å^3.

*Synthesis of [Mn(OIM)(C$_9$H$_{19}$N$_5$)] (**3**).* Compound **1** (0.010 g, 0.031 mmol) was dissolved in 3 mL of tetrahydrofuran followed by the addition of di-*tert*-butyltetrazole (0.017 g, 0.086 mmol), which gave a brown solution. This reaction mixture is stirred for 24−48 h and filtered using a 0.45 PTFE filter and kept in vial containing pentane as

DOI: 10.1021/jacs.8b10250
J. Am. Chem. Soc. 2019, 141, 5699−5709

diffusing solvent at low temperature of −35 °C. Brown needles are obtained after 2 days and isolated by decanting the mother liquor and washing with pentane. Yield: 0.006 g (0.013 mmol), 40% based on compound **1**. CHN combustion analysis indicates low C and N, signifying incomplete combustion. The identity was confirmed by high-resolution mass spectroscopy, and the purity of the crystalline material was confirmed using PXRD (see Supporting Information). ESI-MS: theory, 448.22057; Found, 448.2217. CHN analysis calcd for $C_{10}H_{22}MnN_9$: C, 40.176%; H, 6.968%; N, 40.605%. Found: C, 36.141%, H, 6.545%; N, 38.564%.

*Reaction of [Mn(OIM)(HNtBu)] (**1**) with 2,4,6-Tri-tert-butylphenol.* Compound **1** (0.003g) was dissolved in 1 mL of toluene followed by addition of 0.012 g of solid 2,4,6-tri-*tert*-butylphenol. After 2 h, the reaction was analyzed by EPR spectroscopy for phenoxyl radical.

*Reaction of [Mn(OIM)(HNtBu)] (**1**) with 9,10-dihydroanthracene.* Compound **1** (0.004 g) was dissolved in 2 mL of acetonitrile and followed by the addition of 0.001 g of 9,10-dihydroanthracene, stirred for 24 h in inert atmosphere. The crude reaction mixture was spiked with a known quantity of naphthalene (typically 1.0−2.0 mg weighed on an analytical balance), and this solution was analyzed by gas chromatography.

Density Functional Theoretical Calculations. DFT calculations of both compounds were carried out using the Gaussian G16.A03 software at the M06-2X/6-31G* level of theory for ELF/QTAIM and the MN15/aug-cc-pVTZ level of theory for all other calculations.[77−79] Bond critical points and associated density metrics were determined using the DGrid software,[80] and ELF analysis was conducted using TopMoD.[81−83] Numerical integration for population and localization/delocalization indices were performed with Multiwfn.[84] All calculations were performed on the DoD High Performance Computing Clusters. More details on down selection of computational methods, ELF, and QTAIM analysis are given in the Supporting Information.

■ ASSOCIATED CONTENT

Supporting Information

The Supporting Information is available free of charge on the ACS Publications website at DOI: 10.1021/jacs.8b10250.

UV−visible, EPR, HRMS, and FTIR spectra, gas chromatograms, cyclic voltammograms, XPS fitting, and details of density functional calculations (PDF)

Crystallographic information files for **1**−**3**, also available from CCDC under deposition numbers 1830593, 1830594, and 1830595 (CIF)

Compounds **1** (PDB) and **3** (PDB)

■ AUTHOR INFORMATION

Corresponding Authors

*mzdilla@temple.edu

*jphooper@nps.edu

ORCID

Shivaiah Vaddypally: 0000-0001-6203-9689

Ran Ding: 0000-0003-1894-7369

Megan M. Van Vliet: 0000-0003-1024-4191

Joseph P. Hooper: 0000-0003-4899-1934

Michael J. Zdilla: 0000-0003-0212-2557

Notes

The authors declare no competing financial interest.

■ ACKNOWLEDGMENTS

Support of this work by the Office of Naval Research under award number N00014-16-1-2055 and by the National Science Foundation under award 1362016 is gratefully acknowledged. DFT calculations were supported by the Office of Naval Research Multi-University Research Initiative Grant No. N0001417WX00357. The CENTC elemental analysis center at Rochester University is supported by NSF under award number 0650456. NMR instrumentation at Temple University is supported by a CURE grant from the Pennsylvania Department of Health. The XPS measurements carried out at the University of Delaware surface analysis facility were supported by the NSF under grant 1428149 and by the NIH NIGMS COBRE program under grant P30-GM110758. We thank Anastasia Gallo for assistance with mass spectroscopic measurements. We also thank Ian G. McKendry for helpful discussions about XPS interpretations.

■ REFERENCES

(1) Holley, A. K.; Bakthavatchalu, V.; Velez-Roman, J. M.; St. Clair, D. K. Manganese Superoxide Dismutase: Guardian of the Powerhouse. *Int. J. Mol. Sci.* **2011**, *12*, 7114−7162.

(2) Dau, H.; Zaharieva, I.; Haumann, M. Recent developments in research on water oxidation by photosystem II. *Curr. Opin. Chem. Biol.* **2012**, *16*, 3−10.

(3) Carboni, M.; Latour, J. M. Enzymes with an heterodinuclear iron-manganese active site: Curiosity or necessity? *Coord. Chem. Rev.* **2011**, *255*, 186−202.

(4) Neu, H. M.; Baglia, R. A.; Goldberg, D. P. A Balancing Act: Stability versus Reactivity of Mn(O) Complexes. *Acc. Chem. Res.* **2015**, *48*, 2754−2764.

(5) Eikey, R. A.; Khan, S. I.; Abu-Omar, M. M. The Elusive Terminal Imido of Manganese(V). *Angew. Chem., Int. Ed.* **2002**, *41*, 3591−3595.

(6) Kanady, J. S.; Lin, P.-H.; Carsch, K. M.; Nielsen, R. J.; Takase, M. K.; Goddard, W. A.; Agapie, T. Toward Models for the Full Oxygen-Evolving Complex of Photosystem II by Ligand Coordination To Lower the Symmetry of the Mn3CaO4 Cubane: Demonstration That Electronic Effects Facilitate Binding of a Fifth Metal. *J. Am. Chem. Soc.* **2014**, *136*, 14373−14376.

(7) Chen, J.; Yoon, H.; Lee, Y.-M.; Seo, M. S.; Sarangi, R.; Fukuzumi, S.; Nam, W. Tuning the reactivity of mononuclear nonheme manganese(iv)-oxo complexes by triflic acid. *Chemical Science* **2015**, *6*, 3624−3632.

(8) Yoon, H.; Lee, Y.-M.; Wu, X.; Cho, K.-B.; Sarangi, R.; Nam, W.; Fukuzumi, S. Enhanced Electron-Transfer Reactivity of Nonheme Manganese(IV)−Oxo Complexes by Binding Scandium Ions. *J. Am. Chem. Soc.* **2013**, *135*, 9186−9194.

(9) Gupta, R.; Taguchi, T.; Lassalle-Kaiser, B.; Bominaar, E. L.; Yano, J.; Hendrich, M. P.; Borovik, A. S. High-spin Mn−oxo complexes and their relevance to the oxygen-evolving complex within photosystem II. *Proc. Natl. Acad. Sci. U. S. A.* **2015**, *112*, 5319−5324.

(10) Rivalta, I.; Brudvig, G. W.; Batista, V. S. Oxomanganese complexes for natural and artificial photosynthesis. *Curr. Opin. Chem. Biol.* **2012**, *16*, 11−18.

(11) Reddig, N.; Pursche, D.; Kloskowski, M.; Slinn, C.; Baldeau, S. M.; Rompel, A. Tuning the catalase activity of dinuclear manganese complexes by utilizing different substituted tripodal ligands. *Eur. J. Inorg. Chem.* **2004**, *2004*, 879−887.

(12) Abdolahzadeh, S.; de Boer, J. W.; Browne, W. R. Redox-State Dependent Ligand Exchange in Manganese-Based Oxidation Catalysis. *Eur. J. Inorg. Chem.* **2015**, *2015*, 3432−3456.

(13) Lee, W.-T.; Muñoz, S. B.; Dickie, D. A.; Smith, J. M. Ligand Modification Transforms a Catalase Mimic into a Water Oxidation Catalyst. *Angew. Chem., Int. Ed.* **2014**, *53*, 9856−9859.

(14) Mayer, J. M.; Rhile, I. J.; Larsen, F. B.; Mader, E. A.; Markle, T. F.; DiPasquale, A. G. Models for proton-coupled electron transfer in photosystem II. *Photosynth. Res.* **2006**, *87*, 3−20.

(15) Hammes-Schiffer, S.; Hatcher, E.; Ishikita, H.; Skone, J. H.; Soudackov, A. V. Theoretical studies of proton-coupled electron transfer: Models and concepts relevant to bioenergetics. *Coord. Chem. Rev.* **2008**, *252*, 384−394.

DOI: 10.1021/jacs.8b10250
J. Am. Chem. Soc. 2019, 141, 5699−5709

(16) Mayer, J. M.; Rhile, I. J. Thermodynamics and kinetics of proton-coupled electron transfer: stepwise vs. concerted pathways. *Biochim. Biophys. Acta, Bioenerg.* **2004**, *1655*, 51−58.
(17) Gentry, E. C.; Knowles, R. R. Synthetic Applications of Proton-Coupled Electron Transfer. *Acc. Chem. Res.* **2016**, *49*, 1546−1556.
(18) Dogutan, D. K.; Bediako, D. K.; Graham, D. J.; Lemon, C. M.; Nocera, D. G. Proton-coupled electron transfer chemistry of hangman macrocycles: Hydrogen and oxygen evolution reactions. *J. Porphyrins Phthalocyanines* **2015**, *19*, 1−8.
(19) Yin, P.; Zhang, Q.; Shreeve, J. n. M. Dancing with Energetic Nitrogen Atoms: Versatile N-Functionalization Strategies for N-Heterocyclic Frameworks in High Energy Density Materials. *Acc. Chem. Res.* **2016**, *49*, 4−16.
(20) Fischer, D.; Klapotke, T. M.; Stierstorfer, J. 1,5-Di(nitramino)-tetrazole: High Sensitivity and Superior Explosive Performance. *Angew. Chem., Int. Ed.* **2015**, *54*, 10299−10302.
(21) Heppekausen, J.; Klapotke, T. M.; Sproll, S. A. Synthesis of Functionalized Tetrazenes as Energetic Compounds. *J. Org. Chem.* **2009**, *74*, 2460−2466.
(22) Klapotke, T. M.; Mayer, P.; Schulz, A.; Weigand, J. J. 1,4-bis- 1-methyltetrazol-5-yl −1,4-dimethyl-2-tetrazene: A stable, highly energetic hexamer of diazomethane (CH2N2)(6). *Propellants, Explos., Pyrotech.* **2004**, *29*, 325−332.
(23) Vaddypally, S.; McKendry, I. G.; Tomlinson, W.; Hooper, J. P.; Zdilla, M. J. Electronic Structure of Manganese Complexes of the Redox-Non-innocent Tetrazene Ligand and Evidence for the Metal-Azide/Imido Cycloaddition Intermediate. *Chem. - Eur. J.* **2016**, *22*, 10548−10557.
(24) Gehrmann, T.; Lloret Fillol, J.; Wadepohl, H.; Gade, L. H. Synthesis, Characterization, and Thermal Rearrangement of Zirconium Tetraazadienyl and Pentaazadienyl Complexes. *Organometallics* **2012**, *31*, 4504−4515.
(25) Cramer, S. A.; Hernandez Sanchez, R.; Brakhage, D. F.; Jenkins, D. M. Probing the role of an FeIV tetrazene in catalytic aziridination. *Chem. Commun.* **2014**, *50*, 13967−13970.
(26) Lee, S. W.; Miller, G. A.; Campana, C. F.; Maciejewski, M. L.; Trogler, W. C. Generation of mono- and dianions of 1,4-diphenyl-2-tetrazene by nonoxidative N-N bond formation. A novel route to a 2-tetrazene, a silacyclotetrazene, and the tetrazenide complex (1,4-diphenyltetrazenido)bis(triethylphosphine) palladium. *J. Am. Chem. Soc.* **1987**, *109*, 5050−5051.
(27) King, E. R.; Sazama, G. T.; Betley, T. A. Co(III) Imidos Exhibiting Spin Crossover and C−H Bond Activation. *J. Am. Chem. Soc.* **2012**, *134*, 17858−17861.
(28) Geer, A. M.; Tejel, C.; López, J. A.; Ciriano, M. A. Terminal Imido Rhodium Complexes. *Angew. Chem., Int. Ed.* **2014**, *53*, 5614−5618.
(29) Monillas, W. H.; Yap, G. P. A.; Theopold, K. H. Reactivity of a low-valent chromium dinitrogen complex. *Inorg. Chim. Acta* **2011**, *369*, 103−119.
(30) Danopoulos, A.; Hay-Motherwell, R.; Wilkinson, G.; Cafferkey, S.; Sweet, T.; Hursthouse, M. Reactions of iridium and ruthenium complexes with organic azides. *J. Chem. Soc., Dalton Trans.* **1997**, 3177−3184.
(31) Obenhuber, A. H.; Gianetti, T. L.; Berrebi, X.; Bergman, R. G.; Arnold, J. Reaction of (Bisimido)niobium(V) Complexes with Organic Azides: [3 + 2] Cycloaddition and Reversible Cleavage of β-Diketiminato Ligands Involving Nitrene Transfer. *J. Am. Chem. Soc.* **2014**, *136*, 2994−2997.
(32) Barloy, L.; Gauvin, R. M.; Osborn, J. A.; Sizun, C.; Graff, R.; Kyritsakas, N. Synthesis, Crystal Structure and Solution Behaviour of Palladium(II) Complexes with Tetrazenido or Amido Ligands and Potentially Tridentate Ligands. *Eur. J. Inorg. Chem.* **2001**, *2001*, 1699−1707.
(33) Lee, S. W.; Trogler, W. C. Synthesis, structure, and properties of dicarbonyl bis(phosphine) 1,4-diphenyltetraazabutadiene complexes of molybdenum and tungsten. *Organometallics* **1990**, *9*, 1470−1478.
(34) Michelman, R. I.; Bergman, R. G.; Andersen, R. A. Synthesis, exchange reactions, and metallacycle formation in osmium(II) imido systems: formation and cleavage of osmium-nitrogen bonds. *Organometallics* **1993**, *12*, 2741−2751.
(35) Meyer, K. E.; Walsh, P. J.; Bergman, R. G. A Mechanistic Study of the Cycloaddition-Cycloreversion Reactions of Zirconium-Imido Complex Cp2Zr(N-t-Bu)(THF) with Organic Imines and Organic Azides. *J. Am. Chem. Soc.* **1995**, *117*, 974−985.
(36) Mock, M. T.; Popescu, C. V.; Yap, G. P. A.; Dougherty, W. G.; Riordan, C. G. Monovalent Iron in a Sulfur-Rich Environment. *Inorg. Chem.* **2008**, *47*, 1889−1891.
(37) Bowman, A. C.; Tondreau, A. M.; Lobkovsky, E.; Margulieux, G. W.; Chirik, P. J. Synthesis and Electronic Structure Diversity of Pyridine(diimine)iron Tetrazene Complexes. *Inorg. Chem.* **2018**, *57*, 9634−9643.
(38) Cowley, R. E.; Bill, E.; Neese, F.; Brennessel, W. W.; Holland, P. L. Iron(II) Complexes with Redox-Active Tetrazene (RNNNNR) Ligands. *Inorg. Chem.* **2009**, *48*, 4828−4836.
(39) Jackels, S. C.; Farmery, K.; Barefield, E. K.; Rose, N. J.; Busch, D. H. Tetragonal cobalt(III) complexes containing tetradentate macrocyclic amine ligands with different degrees of unsaturation. *Inorg. Chem.* **1972**, *11*, 2893−2901.
(40) Bakac, A.; Espenson, J. H. Preparation, properties, and crystal structure of a novel series of macrocyclic organocobalt complexes. *Inorg. Chem.* **1987**, *26*, 4353−4355.
(41) Koner, S.; Iijima, S.; Mizutani, F.; Harata, K.; Watanabe, M.; Nagasawa, A.; Sato, M. Fe(III)−azido complex with tetragonally compressed octahedral FeN6 geometry: synthesis, spectroscopic and X-ray single crystal analysis of [Fe(cyclam)(N3)2](ClO4). *Polyhedron* **1999**, *18*, 2201−2204.
(42) Doro, F. G.; Ferreira, K. Q.; da Rocha, Z. N.; Caramori, G. F.; Gomes, A. J.; Tfouni, E. The versatile ruthenium(II/III) tetraazamacrocycle complexes and their nitrosyl derivatives. *Coord. Chem. Rev.* **2016**, *306*, 652−677.
(43) Tfouni, E.; Ferreira, K. Q.; Doro, F. G.; da Silva, R. S.; da Rocha, Z. N. Ru(II) and Ru(III) complexes with cyclam and related species. *Coord. Chem. Rev.* **2005**, *249*, 405−418.
(44) Elias, H. Kinetics and mechanism of metal complex formation with N-4-donor macrocycles of the cyclam type. *Coord. Chem. Rev.* **1999**, *187*, 37−73.
(45) Meyer, M.; Dahaoui-Gindrey, V.; Lecomte, C.; Guilard, L. Conformations and coordination schemes of carboxylate and carbamoyl derivatives of the tetraazamacrocycles cyclen and cyclam, and the relation to their protonation states. *Coord. Chem. Rev.* **1998**, *178*, 1313−1405.
(46) Imler, G. H.; Peters, G. M.; Zdilla, M. J.; Wayland, B. B. Heterobimetallic Complexes of Rhodium Dibenzotetramethylaza-[14]annulene [(tmtaa)Rh-M]: Formation, Structures, and Bond Dissociation Energetics. *Inorg. Chem.* **2015**, *54*, 273−279.
(47) Imler, G. H.; Zdilla, M. J.; Wayland, B. B. Equilibrium Thermodynamics To Form a Rhodium Formyl Complex from Reactions of CO and H2: Metal σ Donor Activation of CO. *J. Am. Chem. Soc.* **2014**, *136*, 5856−5859.
(48) Imler, G. H.; Zdilla, M. J.; Wayland, B. B. Evaluation of the Rh(II)−Rh(II) Bond Dissociation Enthalpy for [(TMTAA)Rh]2 by 1H NMR T2Measurements: Application in Determining the Rh−C(O)− BDE in [(TMTAA)Rh]2C = O. *Inorg. Chem.* **2013**, *52*, 11509−11513.
(49) Franceschi, F.; Hesschenbrouck, J.; Solari, E.; Floriani, C.; Re, N.; Rizzoli, C.; Chiesi-Villa, A. The reactivity of dibenzotetramethyltetraaza 14 annulene-Mn(II): functionalisation of manganese in a macrocyclic environment. *J. Chem. Soc., Dalton Trans.* **2000**, 593−604.
(50) Sakata, K.; Wang, Z. L.; Hashimoto, M.; Tsuge, A.; Tanoue, Y. Characterization, spectroscopic properties and crystal structure of a tetraaza 14 annulene manganese(III) complex. *Synth. React. Inorg. Met.-Org. Chem.* **1999**, *29*, 265−277.
(51) Weiss, M. C.; Bursten, B.; Peng, S.-M.; Goedken, V. L. Effects of peripheral steric constraints and metal ion size on the structure of three five-coordinate macrocyclic ligand complexes of the type

DOI: 10.1021/jacs.8b10250
J. Am. Chem. Soc. 2019, 141, 5699−5709

[M(C22H22N4)X], M = cobalt(III), iron(III), manganese(II); X = iodine, chlorine, triethylamine. *J. Am. Chem. Soc.* **1976**, *98*, 8021−8031.
(52) Caiut, J.; Nakagaki, S.; Friedermann, G. R.; Drechsel, S. M.; Zarbin, A. J. G. Nickel(II) and manganese(III) tetraazaannulenes complexes encapsulated in porous Vycor glass (PVG): investigation of catalytic activity. *J. Mol. Catal. A: Chem.* **2004**, *222*, 213−222.
(53) Caiut, J. M. A.; Nakagaki, S.; Friedermann, G. R.; Franca, R. A.; Zarbin, A. J. G. Synthesis and characterization of nickel(II) and manganese(III) complexes of tetraazaannulene and encapsulation in porous Vycor glass (PVG). *J. Inorg. Biochem.* **2001**, *86*, 166−166.
(54) McCall, J. D.; Vaddypally, S.; Kondaveeti, S. K.; Zdilla, M. J. Easy access to the Wilkinson tris(tert-butylimido)nitridomanganate-(VII) complex from commercially available starting materials. *Inorg. Chem. Commun.* **2013**, *37*, 225−227.
(55) Kondaveeti, S. K.; Vaddypally, S.; McCall, J. D.; Zdilla, M. J. Electronic structure and solution behavior of a tris(N,N[prime or minute]-diphenylhydrazido)manganese(iv) propeller complex. *Dalton Trans* **2012**, *41*, 8093−8097.
(56) LoCoco, M. D.; Zhang, X.; Jordan, R. F. Chelate-Controlled Synthesis of Racemic ansa-Zirconocenes. *J. Am. Chem. Soc.* **2004**, *126*, 15231−15244.
(57) Andersen, R. A.; Faegri, K.; Green, J. C.; Haaland, A.; Lappert, M. F.; Leung, W. P.; Rypdal, K. Synthesis of bis[bis(trimethylsilyl)-amido]iron(II). Structure and bonding in M[N(SiMe3)2]2 (M = manganese, iron, cobalt): two-coordinate transition-metal amides. *Inorg. Chem.* **1988**, *27*, 1782−1786.
(58) Luca, O. R.; Crabtree, R. H. Redox-active ligands in catalysis. *Chem. Soc. Rev.* **2013**, *42*, 1440−1459.
(59) Butschke, B.; Fillman, K. L.; Bendikov, T.; Shimon, L. J. W.; Diskin-Posner, Y.; Leitus, G.; Gorelsky, S. I.; Neidig, M. L.; Milstein, D. How Innocent are Potentially Redox Non-Innocent Ligands? Electronic Structure and Metal Oxidation States in Iron-PNN Complexes as a Representative Case Study. *Inorg. Chem.* **2015**, *54*, 4909−4926.
(60) Baglia, R. A.; Prokop-Prigge, K. A.; Neu, H. M.; Siegler, M. A.; Goldberg, D. P. Mn(V)(O) versus Cr(V)(O) Porphyrinoid Complexes: Structural Characterization and Implications for Basicity Controlling H-Atom Abstraction. *J. Am. Chem. Soc.* **2015**, *137*, 10874−10877.
(61) Hill, C. L.; Hollander, F. J. Structural characterization of a complex of Manganese(V) nitrido[tetrakis(p-methoxyphenyl)-porphinato] manganese(V). *J. Am. Chem. Soc.* **1982**, *104*, 7318−7319.
(62) Miller, C. G.; Gordon-Wylie, S. W.; Horwitz, C. P.; Strazisar, S. A.; Peraino, D. K.; Clark, G. R.; Weintraub, S. T.; Collins, T. J. A Method for Driving O-Atom Transfer: Secondary Ion Binding to a Tetraamide Macrocyclic Ligand. *J. Am. Chem. Soc.* **1998**, *120*, 11540−11541.
(63) Meyer, K.; Bendix, J.; Metzler-Nolte, N.; Weyhermüller, T.; Wieghardt, K. Nitridomanganese(V) and -(VI) Complexes Containing Macrocyclic Amine Ligands. *J. Am. Chem. Soc.* **1998**, *120*, 7260−7270.
(64) Buchler, J. W.; Dreher, C.; Lay, K. L.; Lee, Y. J.; Scheidt, W. R. Metal complexes with tetrapyrrole ligands. 30. The manganese-nitrogen triple bond. Synthesis and molecular stereochemistry of (5,15-dimethyl-2,3,7,8,12,13,17,18-octaethyl-5H,15H-porphinato)-nitridomanganese(V). *Inorg. Chem.* **1983**, *22*, 888−891.
(65) Zdilla, M. J.; Abu-Omar, M. M. Mechanism of Catalytic Aziridination with Manganese Corrole: The Often Postulated High-Valent Mn(V) Imido Is Not the Group Transfer Reagent. *J. Am. Chem. Soc.* **2006**, *128*, 16971−16979.
(66) Lansky, D. E.; Mandimutsira, B.; Ramdhanie, B.; Clausén, M.; Penner-Hahn, J.; Zvyagin, S. A.; Telser, J.; Krzystek, J.; Zhan, R.; Ou, Z.; Kadish, K. M.; Zakharov, L.; Rheingold, A. L.; Goldberg, D. P. Synthesis, Characterization, and Physicochemical Properties of Manganese(III) and Manganese(V)−Oxo Corrolazines. *Inorg. Chem.* **2005**, *44*, 4485−4498.
(67) Biesinger, M. C.; Payne, B. P.; Grosvenor, A. P.; Lau, L. W. M.; Gerson, A. R.; Smart, R. S. C. Resolving surface chemical states in XPS analysis of first row transition metals, oxides and hydroxides: Cr, Mn, Fe, Co and Ni. *Appl. Surf. Sci.* **2011**, *257*, 2717−2730.
(68) Gostynski, R.; Conradie, J.; Erasmus, E. Significance of the electron-density of molecular fragments on the properties of manganese(iii) β-diketonato complexes: an XPS and DFT study. *RSC Adv.* **2017**, *7*, 27718−27728.
(69) Walter, C.; Menezes, P. W.; Orthmann, S.; Schuch, J.; Connor, P.; Kaiser, B.; Lerch, M.; Driess, M. A Molecular Approach to Manganese Nitride Acting as a High Performance Electrocatalyst in the Oxygen Evolution Reaction. *Angew. Chem., Int. Ed.* **2018**, *57*, 698−702.
(70) Nesbitt, H. W.; Canning, G. W.; Bancroft, G. M. XPS study of reductive dissolution of 7Å-birnessite by H3AsO3, with constraints on reaction mechanism. *Geochim. Cosmochim. Acta* **1998**, *62*, 2097−2110.
(71) Cerrato, J. M.; Hochella, M. F.; Knocke, W. R.; Dietrich, A. M.; Cromer, T. F. Use of XPS to Identify the Oxidation State of Mn in Solid Surfaces of Filtration Media Oxide Samples from Drinking Water Treatment Plants. *Environ. Sci. Technol.* **2010**, *44*, 5881−5886.
(72) Caffarel, M.; Giner, E.; Scemama, A.; Ramírez-Solís, A. Spin Density Distribution in Open-Shell Transition Metal Systems: A Comparative Post-Hartree−Fock, Density Functional Theory, and Quantum Monte Carlo Study of the CuCl2Molecule. *J. Chem. Theory Comput.* **2014**, *10*, 5286−5296.
(73) Harvey, J. N. DFT Computation of Relative Spin-State Energetics of Transition Metal Compounds. In *Principles and Applications of Density Functional Theory*; Inorganic Chemistry I. Structure and Bonding; Springer: Berlin, Heidelberg, 2004; Vol. *112*.
(74) Savin, A.; Nesper, R.; Wengert, S.; Fassler, T. F. ELF: The electron localization function. *Angew. Chem., Int. Ed. Engl.* **1997**, *36*, 1808−1832.
(75) Voitekhovich, S. V.; Gaponik, P. N.; Lyakhov, A. S.; Ivashkevich, O. A. Endo- and exocyclic N-alkylation of 1- and 5-aminotetrazoles with t-BuOH−HClO4: synthesis of mono-, di-, and tri-tert-butyl substituted aminotetrazolium salts. *Tetrahedron* **2008**, *64*, 8721−8725.
(76) Lucarini, M.; Pedrielli, P.; Pedulli, G. F.; Cabiddu, S.; Fattuoni, C. Bond Dissociation Energies of O−H Bonds in Substituted Phenols from Equilibration Studies. *J. Org. Chem.* **1996**, *61*, 9259−9263.
(77) Sun, Q. A.; Wang, J. T.; Zhang, L. M.; Yang, M. P. Photoinduced Electron and Hydrogen Transfer Reactions of Thioxanthone with Amines, Phenols and Alcohols. *Acta Phys.-Chim. Sin.* **2010**, *26*, 2481−2488.
(78) Kim, S. S.; Kim, M.; Kang, H. Effects of Amino Substitution on the Excited State Hydrogen Transfer in Phenol: A TDDFT Study. *Bull. Korean Chem. Soc.* **2009**, *30*, 1481−1484.
(79) Amorati, R.; Menichetti, S.; Mileo, E.; Pedulli, G. F.; Viglianisi, C. Hydrogen-Atom Transfer Reactions from ortho-Alkoxy-Substituted Phenols: An Experimental Approach. *Chem. - Eur. J.* **2009**, *15*, 4402−4410.
(80) Nielsen, M. F.; Ingold, K. U. Kinetic solvent effects on proton and hydrogen atom transfers from phenols. Similarities and differences. *J. Am. Chem. Soc.* **2006**, *128*, 1172−1182.
(81) MacFaul, P. A.; Ingold, K. U.; Lusztyk, J. Kinetic solvent effects on hydrogen atom abstraction from phenol, aniline, and diphenylamine. The importance of hydrogen bonding on their radical-trapping (antioxidant) activities. *J. Org. Chem.* **1996**, *61*, 1316−1321.
(82) Hull, J. F.; Balcells, D.; Sauer, E. L. O.; Raynaud, C.; Brudvig, G. W.; Crabtree, R. H.; Eisenstein, O. Manganese Catalysts for C−H Activation: An Experimental/Theoretical Study Identifies the Stereoelectronic Factor That Controls the Switch between Hydroxylation and Desaturation Pathways. *J. Am. Chem. Soc.* **2010**, *132*, 7605−7616.
(83) Zaragoza, J. P. T.; Siegler, M. A.; Goldberg, D. P. A Reactive Manganese(IV)-Hydroxide Complex: A Missing Intermediate in Hydrogen Atom Transfer by High-Valent Metal-Oxo Porphyrinoid Compounds. *J. Am. Chem. Soc.* **2018**, *140*, 4380−4390.
(84) Rice, D. B.; Massie, A. A.; Jackson, T. A. Manganese-Oxygen Intermediates in O-O Bond Activation and Hydrogen-Atom Transfer Reactions. *Acc. Chem. Res.* **2017**, *50*, 2706−2717.

DOI: 10.1021/jacs.8b10250
J. Am. Chem. Soc. 2019, 141, 5699−5709

(85) Garcia-Bosch, I.; Company, A.; Cady, C. W.; Styring, S.; Browne, W. R.; Ribas, X.; Costas, M. Evidence for a Precursor Complex in C-H Hydrogen Atom Transfer Reactions Mediated by a Manganese(IV) Oxo Complex. *Angew. Chem., Int. Ed.* **2011**, *50*, 5648−5653.
(86) Goldsmith, C. R.; Cole, A. P.; Stack, T. D. P. C-H activation by a mononuclear manganese(III) hydroxide complex: Synthesis and characterization of a manganese-lipoxygenase mimic? *J. Am. Chem. Soc.* **2005**, *127*, 9904−9912.
(87) Ni, C. B.; Fettinger, J. C.; Power, P. P. Intramolecular C-H Activation by Putative Terminal Two-Coordinate Manganese(III) Imido Intermediates: Hydrogen Abstraction from a Phenyl Group. *Organometallics* **2010**, *29*, 269−272.
(88) Zdilla, M. J.; Abu-Omar, M. M. Manganese(III) Corrole-Oxidant Adduct as the Active Intermediate in Catalytic Hydrogen Atom Transfer. *Inorg. Chem.* **2008**, *47*, 10718−10722.
(89) Zdilla, M. J.; Dexheimer, J. L.; Abu-Omar, M. M. Hydrogen atom transfer reactions of imido manganese(V) corrole: One reaction with two mechanistic pathways. *J. Am. Chem. Soc.* **2007**, *129*, 11505−11511.
(90) Rapta, P.; Brezova, V.; Ceppan, M.; Melnik, M.; Bustin, D.; Stasko, A. Radical Intermediates in the Redox Reactions of Tetrazolium Salts in Aprotic Solvents-(Cyclovoltammetric, EPR, and UV-Vis Study). *Free Radical Res.* **1994**, *20*, 71−82.
(91) Podenko, L. S.; Chirkov, A. K.; Shchipanov, V. P. An Electron-Paramagnetic-Res Study of Isotropic HFI In Tetrazolyl Radicals. *J. Struct. Chem.* **1982**, *23*, 161−163.
(92) Podenko, L. S.; Chirkov, A. K.; Shchipanov, V. P. Electron-Spin-Resonance Spectra and Structure of Tetrazolyl Radicals. *J. Struct. Chem.* **1983**, *23*, 559−564.
(93) Cortes-Guzman, F.; Bader, R. F. W. Complementarity of QTAIM and MO theory in the study of bonding in donor-acceptor complexes. *Coord. Chem. Rev.* **2005**, *249*, 633−662.
(94) Zaragoza, J. P. T.; Siegler, M. A.; Goldberg, D. P. Rhenium(v)−oxo corrolazines: isolating redox-active ligand reactivity. *Chem. Commun.* **2016**, *52*, 167−170.
(95) Leeladee, P.; Baglia, R. A.; Prokop, K. A.; Latifi, R.; de Visser, S. P.; Goldberg, D. P. Valence Tautomerism in a High-Valent Manganese-Oxo Porphyrinoid Complex Induced by a Lewis Acid. *J. Am. Chem. Soc.* **2012**, *134*, 10397−10400.
(96) Bougher, C. J.; Abu-Omar, M. M. Lewis-Acid-assisted Hydrogen Atom Transfer to Manganese(V)-Oxo Corrole through Valence Tautomerization. *ChemistryOpen* **2016**, *5*, 522−524.
(97) Bruker. *COSMO, SAINT, SADABS. COSMO, SAINT, SADABS*; Bruker AXS Inc.: Madison, WI, 2008.
(98) Sheldrick, G. M. A short history of SHELX. *Acta Crystallogr., Sect. A: Found. Crystallogr.* **2008**, *A64*, 112−122.
(99) Dolomanov, O. V.; Bourhis, L. J.; Gildea, R. J.; Howard, J. A. K.; Puschmann, H. OLEX2: a complete structure solution, refinement and analysis program. *J. Appl. Crystallogr.* **2009**, *42*, 339−341.
(100) Gupta, R. P.; Sen, S. K. Calculation of multiplet structure of core p-vacancy levels II. *Phys. Rev. B* **1975**, *12*, 15−19.
(101) Gupta, R. P.; Sen, S. K. Calculation of multiplet structure of core p-vacancy levels. *Phys. Rev. B* **1974**, *10*, 71−77.

DOI: 10.1021/jacs.8b10250
J. Am. Chem. Soc. 2019, 141, 5699−5709